ACS APPLIED NANO MATERIALS

www.acsanm.org Article

Computational Study on Strain-Engineered Graphene Nanopores for Selective Gas Separation

Enlai Gao,* Chunbo Zhang, Ke Zhou, and Ning Wei*

Cite This: *ACS Appl. Nano Mater.* 2020, 3, 11474−11480 Read Online

ACCESS | Metrics & More | Article Recommendations | Supporting Information

ABSTRACT: Precise fine-tuning of gas transport across nanopores is highly desirable in numerous industrial applications. In this work, we perform a computational study to investigate the strain engineering of gas permeation across the nanopores in graphene. First, we optimize the geometries of nanoporous graphene under uniaxial and biaxial strains using first-principles calculations and thus compute the potential energy barriers for gases (He, H_2, O_2, CO, CO_2, and N_2) across these nanopores. Afterward, the capability of the strain-engineered nanopores for selective gas separation is accessed based on the computations and transition state theory. Our calculations demonstrate that the strain-engineered nanopores exhibit remarkably improved permeance while maintaining significant selectivity for gas separation, yielding as high as 34 orders of magnitude increase in the gas transport rate. Finally, the underlying mechanism of the mechanosensitive nanopores for selective gas separation gas is revealed by providing insight into the atomic and electronic structures. Our findings shed light on strain engineering permeance and selectivity of nanopores in two-dimensional materials.

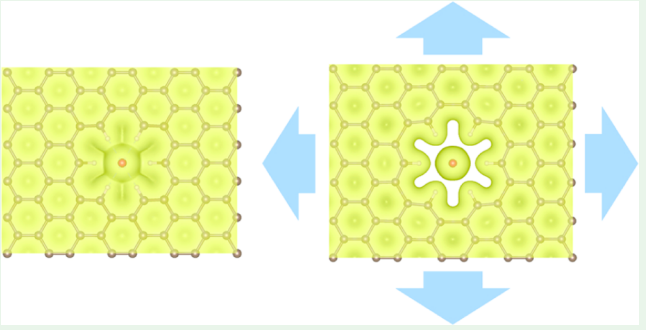

KEYWORDS: *nanopores, gas separation, strain engineering, permeance, selectivity*

1. INTRODUCTION

Gas separation plays an essential role in energy and technological applications.[1] The well-known examples include the separation of H_2/CO for hydrogen fuel production,[2] the purification of He from natural gas,[3] and CO_2/N_2 separation for greenhouse gas capture.[4] In the past decades, various separation technologies have experienced fast increases, and a large number of materials, such as carbon molecular sieves, silica, porous polymers, and metal−organic framework, have been developed for gas separations.[5−10] However, the development of new-generation membranes with optimal permeance and selectivity is continuously driven by the increasing industrial demands.[11,12]

The permeance of a membrane is inversely proportional to the membrane thickness, and hence the common bulk membranes with considerable thickness are limited in their efficiency. The existing studies of membrane-based gas separation demonstrate that thin membranes with fine pores boast a synergy of high permeance and high selectivity, resulting from a reduced transport distance and precise size-exclusion separation of the gases. Hence, two-dimensional materials of atom thick, such as graphene and graphene-like two-dimensional materials, hold a great promise for efficient mass separation,[13−17] among which graphene is a perfect testbed for probing the fundamental separation properties of atom-thick membranes.[14] However, defect-free graphene is impermeable to gases[18,19] because the electron density of the aromatic rings in graphene is so dense that no atoms can pass through these rings. Therefore, it is necessary to fabricate nanoporous graphene by introducing defects, such as the Stone−Wales[20] and vacancy defects,[21] to achieve gas permeability. Many experimental technologies, such as oxygen plasma irradiation,[22] ultraviolet-oxidative etching,[23] and carbothermal reactions with metal nanoparticles,[24] have been developed to produce defects. Meanwhile, two-dimensional materials with intrinsic pores, such as graphdiyne[25] and two-dimensional metal−organic frameworks,[26] can also be used for gas separation. The permeance and selectivity of the atom-thick membranes are determined by the shape and size of nanopores that are usually formed in the fabrication, which, however, are usually not optimal for separating various gases. Therefore, the tuning of the nanopores for efficient gas separation is highly desirable.

It is known that strain engineering is widely used for tuning the structure and properties of materials.[27−29] In this work, we

Received: September 24, 2020
Accepted: October 23, 2020
Published: November 9, 2020

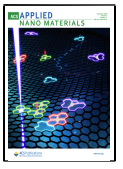

https://dx.doi.org/10.1021/acsanm.0c02340
ACS Appl. Nano Mater. 2020, 3, 11474−11480

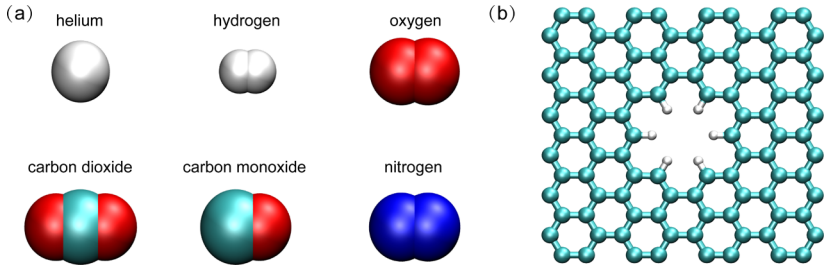

Figure 1. Atomic structures of (a) typical gas molecules and (b) a hydrogen-passivated nanopore in graphene.

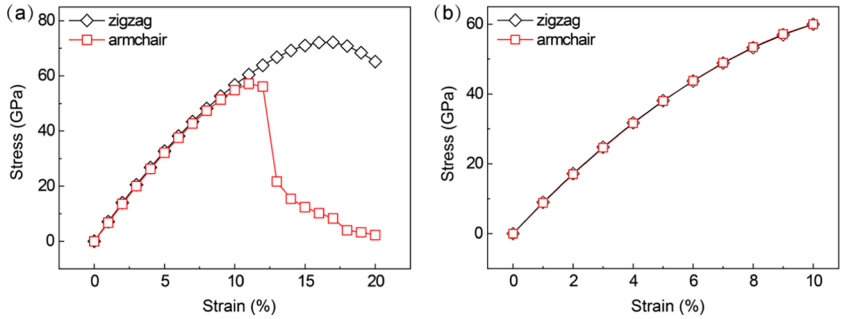

Figure 2. Mechanical response of nanoporous graphene under (a) uniaxial and (b) biaxial loadings.

investigate the gas separation performance of strain-engineered graphene nanopores based on the first-principles calculations and transition state theory. We compute the potential energy barriers for gases (He, H_2, O_2, CO, CO_2, and N_2) passing through graphene nanopores under uniaxial and biaxial strains and then assess their capability for selective gas separation. It is found that the graphene nanopore exhibits highly mechano-sensitive permeance of gases, suggesting that the strain engineering strategy could be used to precisely tune the gas transport across nanopores. The mechanism of the mechano-sensitive gas transport is elucidated by tracking the evolution of atomic and electronic structures with the increasing strain.

2. COMPUTATIONAL MODELS AND METHODS

First-principles calculations, as implemented in the Vienna *ab-initio* simulation package (VASP),[30,31] are performed to investigate the gas separation performance of strain-engineered nanopores. The electron−core interactions are treated by the projector-augmented wave (PAW) method within the frozen core approximation,[32] and the exchange-correlation interactions between electrons are described by generalized gradient approximation (GGA) functional parameterized by Perdew, Burke, and Ernzerhof (PBE).[33] Unless otherwise noted, the adopted energy cutoff is 520 eV, and the *k*-points mesh used is 2×2×1 for the calculations.[34] It is noted here that the energy cutoff of 620 eV is adopted for He atoms because of its high default value. Considering the dispersion interactions, we employ van der Waals correction using the DFT-D3 method.[35] The atom positions and lattice parameters are energy minimized until the force tolerance of 0.01 eV/Å. To avoid the interactions between the periodic replicas, a vacuum separation of 30 Å is adopted. Additionally, spin-polarized calculations were adopted for simulations containing oxygen molecules.

The initial structures of a hydrogen-passivated nanopore in graphene and free gases (He, H_2, O_2, CO, CO_2, and N_2) are optimized using a conjugate gradient algorithm (Figure 1). Without loss of generality, the experimentally observed graphene nanopore made by missing six carbon atoms and functionalized with hydrogen was adopted to introduce the concept of strain-engineered nanopores for selective gas separation. It is expected that this concept can be generalized to other pores with different shapes and sizes. The optimized geometries of gas molecules agree with the literature reports (Table S1). Afterward, the climbing image nudged elastic band (CI-NEB) method is used to calculate the potential energy of gases passing through the nanopore.[36] In all CI-NEB calculations, five images are used between the optimized initial and final states, which will be discussed later. The nanoporous graphene was flexible during the simulations. Finally, the energy barriers of gases are derived from the transition paths, which are then used to determine the permeance of gases based on the transition state theory.

3. RESULTS AND DISCUSSION

3.1. Structural Integrity of Nanoporous Graphene under Mechanical Perturbation. In the computation, an optimized supercell of free-standing graphene consisting of a hydrogen-passivated nanopore exhibits sizes of 12.87 Å × 12.39 Å, which are 0.3 and 0.4% larger than that calculated for defect-free graphene. The discrepancy in the lattice constants is due to the existing nanopore in graphene that enlarges the structure.

Before investigating the gas transport behaviors across the nanoporous graphene, we first characterize the structural integrity of the nanoporous graphene. Figure 2 shows the calculated stress−strain curves of graphene under uniaxial and biaxial strains. Herein, nominal strain and stress are used, which are defined as the length change divided by the original length and the tensile force divided by the original area of cross section, respectively (nominal thickness of 3.4 Å is adopted). Figure 2a shows that the mechanical responses of nanoporous graphene stretched along the armchair direction become distinct from that along the zigzag direction with the increasing strain, resulting from the strain-induced symmetry breaking. The strain to failure of this nanoporous graphene loaded along the armchair and zigzag directions are 11 and 17%, respectively, which defines the maximum strains that can be applied to the structure. In addition to uniaxial strain, we also investigate the elastic responses of biaxial strain, and the strain to failure can also exceed 10% (Figure 2b). Considering the structural stability based on these investigations, we explore the

https://dx.doi.org/10.1021/acsanm.0c02340
ACS Appl. Nano Mater. 2020, 3, 11474−11480

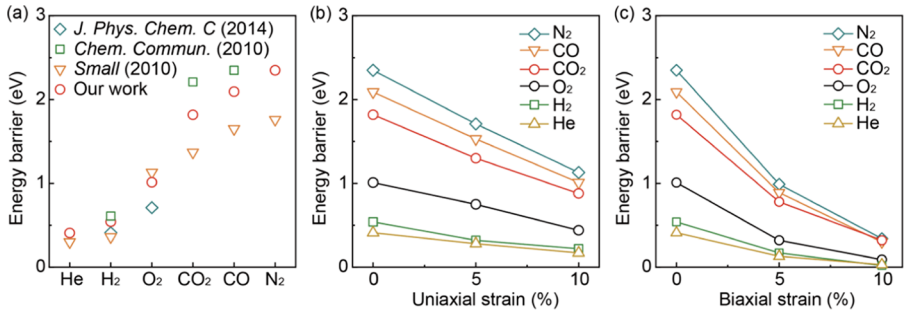

Figure 3. (a) Energy barriers of gas molecules across the nanopore in graphene. The literature data are from Ambrosetti et al.,[38] Li et al.,[40] and Blankenburg et al..[39] Energy barriers of gas molecules across the nanopore in graphene under (b) uniaxial strain and (c) biaxial strain.

gas separation performance of nanoporous graphene under uniaxial and biaxial strains below 10%.

3.2. Strain Engineering Gas Separation Performance of Nanoporous Graphene. To investigate the permeability and selectivity of the nanoporous graphene for gas separation, we calculate the minimum-energy pathway of gas molecules across the nanoporous graphene. The energy barrier (ΔE) is defined as the largest energy difference between a local minimum and any subsequent local maximum during the crossing of barrier[37]

$$\Delta E = E_{TS} - E_{SS} \quad (1)$$

where E_{TS} and E_{SS} are the total energy of the transition state of gas across the nanoporous graphene and the stable state (SS) of gas across the nanoporous graphene, respectively.

To balance the computational efficiency and accuracy, we test the number of images in the CI-NEB calculations of gas molecules across the graphene nanopore. Two initial configurations for calculating the energy pathway of He across the nanoporous graphene are constructed, in which the He atoms are 3.0 and 6.0 Å from graphene before optimization. After optimization, the initial height of 3.0 Å slightly changes to the optimal adsorption height while the initial height of 6.0 Å almost does not change, and 5 and 19 images are used for these two structures, respectively. The energy profiles of He atom across the graphene nanopore is shown in Figure S1, from which we calculate the energy barriers of He passing through these two structures as 0.4069 and 0.4072 eV, respectively, showing a very tiny difference (0.07%). Hence, five images for the CI-NEB calculations are adopted for a balance between computational accuracy and efficiency. Figure 3 demonstrates that the energy barriers are 0.41, 0.54, 1.01, 1.82, 2.09, and 2.35 eV for He, H_2, O_2, CO_2, CO, and N_2, respectively, which agrees with the literature reports.[38−40] In comparison, the order of increasing kinetic diameter of gas molecules is He (2.55 Å), H_2 (2.89 Å), CO_2 (3.30 Å), O_2 (3.47 Å), N_2 (3.64 Å), and CO (3.69 Å).[41,42] The quite low energy barriers of He (0.41 eV) and H_2 (0.54 eV) suggest that they can pass through the graphene nanopore at moderate temperature and pressure. However, the permeation of O_2, CO, CO_2, or N_2 through the graphene nanopore is hindered because of their high energy barriers. The slight mismatch between the physical kinetic diameter and energy barriers of gases suggests that other factors, such as geometries and chemical interactions, also matter during the gas permeation.[39] Subsequently, we calculate the potential energy barriers of gases passing through the nanoporous graphene under uniaxial strains of 5% and 10% along the armchair direction and biaxial strains of 5% and 10%, respectively, which are summarized in Table S2. In general, it can be found that the energy barriers of all gases decrease with the increasing of uniaxial or biaxial strains, and the biaxial loading more significantly reduces the energy barriers compared with uniaxial loading at the same magnitude of strains. For example, the energy barrier of hydrogen can be reduced to 3.70% of its original value in these ranges of mechanical strains, indicating the mechanosensitive permeance of gases through the nanoporous membrane.

To quantify the efficiency of the gas separation, the Arrhenius equation[43] is used to estimate the transport rate of the gas molecule across the graphene nanopore. The Arrhenius equation is written as

$$R = A \exp(-\Delta E/k_B T) \quad (2)$$

where R is the transport rate, A is the pre-exponential factor, k_B is the Boltzmann constant, and T is the temperature. Herein, the potential effects of the pressure and reverse migration on eq 2 are discussed. The two parts are energy barrier and pre-exponential factor in eq 2. The contribution of pressure on the energy barrier can be estimated by $\Delta E_p = \Delta P \times \Delta x \times \Delta S$, where ΔP is the pressure difference between the feed and the permeate side (usually ~<100 bar in the experiments), Δx is the migration distance along the nanopores (on the order of interlayer distance of graphene ~3.4 Å), and ΔS is the area of nanopores (~2−5 Å^2 in our work). The calculated $\Delta E_p \ll 0.1$ eV is much smaller than the calculated translation energy barriers. On the other hand, the pre-exponential factor is not pressure-dependent but depends on the gas types and pore configurations.[44] Thus, the effects of the pressure on eq 2 is expected to be negligible. As for the back migration, the difference in partial pressure between the feed side and the permeate side is usually very large, and hence the effect of back migration was also neglected.

Furthermore, to investigate the effect of mechanical loading on gas permeance through nanoporous graphene, the relative transport rates of gas through strained nanopore compared with that through strain-free nanopore can be expressed as

$$P_{X/X_{strain=0}} = \frac{A\, e^{-\Delta E_X/k_B T}}{A\, e^{-\Delta E_0/k_B T}} = e^{(\Delta E_0 - \Delta E_X)/k_B T} \quad (3)$$

where we assume that the prefactors are identical for all gases as used in the previous work[39,42,45] and ΔE_X and ΔE_0 are the energy barriers of gas passing through straining nanopores and strain-free nanopores. The ratio characterizes the enhanced transport rate of nanoporous graphene upon mechanical loadings. The transport rates for various gases across the nanoporous graphene under different strains are shown in Figure 4. It can be found that $P_{X/X_{strain=0}}$ almost linearly increases

https://dx.doi.org/10.1021/acsanm.0c02340
ACS Appl. Nano Mater. 2020, 3, 11474−11480

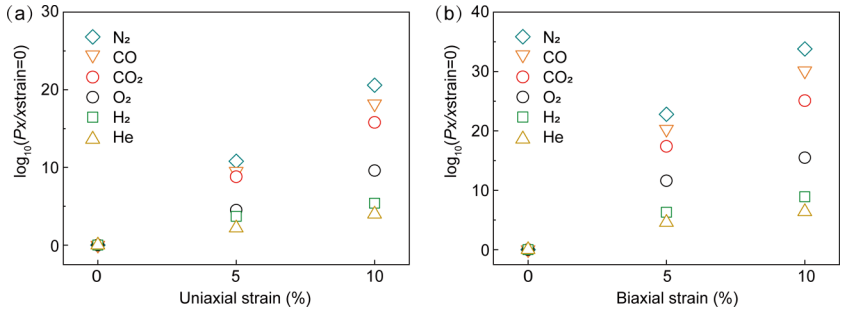

Figure 4. Logarithmic scale for the relative gas transport rates of nanoporous graphene under (a) uniaxial strains and (b) biaxial strains.

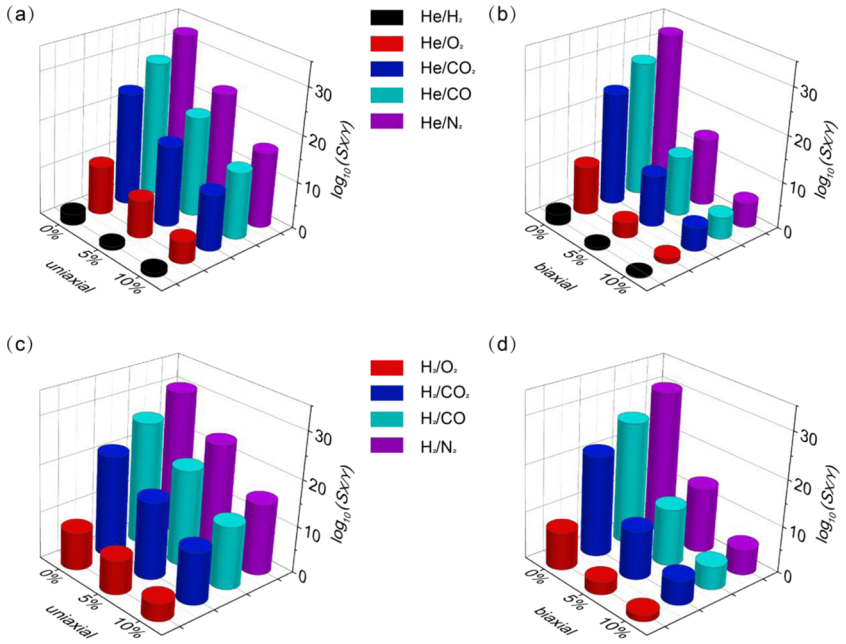

Figure 5. Logarithmic scale for the selectivities of nanoporous graphene in separating (a, b) He and (c, d) H_2 from other gases under uniaxial and biaxial loadings, respectively.

with the increase of uniaxial and biaxial strains. In general, the slopes of the increasing trend are higher for gases with larger energy barriers. Notably, the energy barriers of O_2, CO_2, CO, and N_2 can be reduced from their original values of 1.01, 1.82, 2.09, and 2.35 eV before strain engineering to as low as 0.09, 0.32, 0.30, and 0.34 eV after strain engineering, respectively (Figure 3b,c). As a consequence, the relative permeation rate can increase by as high as 34 orders of magnitude, indicating the mechanosensitivity (Figure 4).

Finally, the effect of mechanical loading on the gas selectivity of nanoporous graphene is investigated. Based on the Arrhenius equation, the selectivity is defined as the transport rate of H_2/He relative to that of other common gases (O_2, CO, CO_2, and N_2). To be specific, the selectivity for gas pair (X/Y) is the ratio between the transport rates of gas X and gas Y (r_X and r_Y)

$$S_{X/Y} = \frac{r_X}{r_Y} = \frac{A_X\, e^{-\Delta E_X/k_B T}}{A_Y\, e^{-\Delta E_Y/k_B T}} \quad (4)$$

where A is the prefactor, k_B is the Boltzmann constant, and T is the temperature. For simplicity, we assume that the prefactors are identical for all gases as used in the previous work.[39,42,45] Herein, it should be noted here that this assumption neglects the entropic contributions that promote the transport of smaller, more spherical gas molecules and inhibit the transport of larger, more elongated gas molecules.[46] Hence, this assumption results in a slight underestimation of the selectivity for separating smaller gas molecules out of larger gas molecules. The selectivities for typical gas pairs are shown in Figure 5, from which we can find that the selectivities in the separation of He and H_2 from other gases both decrease with the increase in uniaxial and biaxial strains. However, it should be noted that there are some applied strains that make the nanopores exhibit remarkably improved permeance while maintaining significant selectivity for gas separation (Figures 4 and 5). To achieve the balance between the permeation and the selectivity for specific gas pairs in practical uses, the applied strain to the nanoporous graphene should be optimized.

3.3. Mechanism Discussion. To explain the fundamental interaction between gas molecules and graphene, the diameter of the graphene nanopore was calculated. As proposed by Jiang et al.,[21] the key factor in the separation of small gas molecules is the nanopore size relative to the kinetic radii of the target molecules. The aim of strain-engineered graphene nanopore is to make the transport of other molecules dynamically unfavorable while maintaining the selective transport of target molecules. To elucidate the essential physics behind the significant tunability of gas separation performance of nano-

https://dx.doi.org/10.1021/acsanm.0c02340
ACS Appl. Nano Mater. 2020, 3, 11474−11480

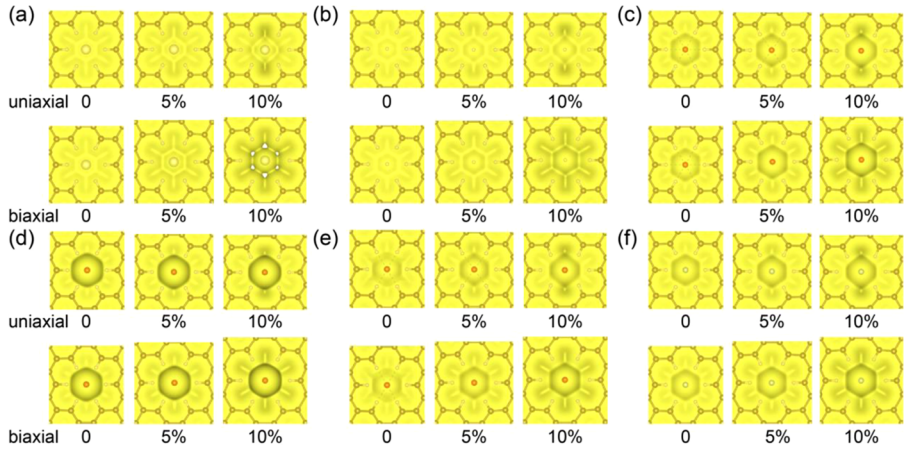

Figure 6. Electron density distributions of (a) He, (b) H_2, (c) O_2, (d) CO_2, (e) CO, and (f) N_2 passing through the strain-engineered graphene nanopores at the transition state, respectively, in which the isosurface value is adopted as 0.02 e/Å^3.

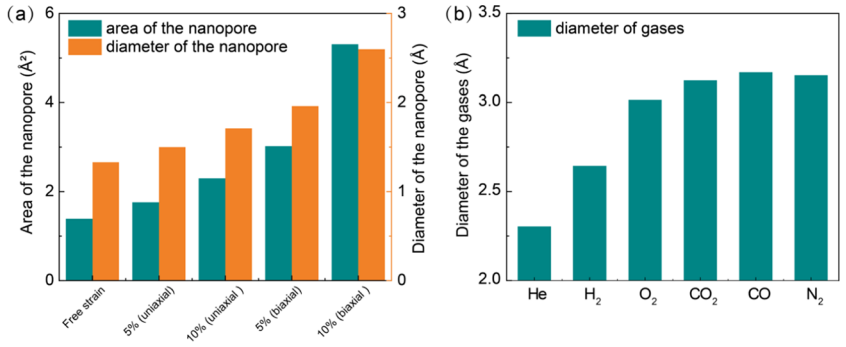

Figure 7. Sizes of nanopores (a) and gases (b) calculated from their electron density distributions, in which the isosurface value is adopted as 0.02 e/Å^3.

porous graphene by strain engineering, we study the microstructure evolution of the nanopore in graphene based on computational evidence. Specifically, the electron density distribution for the transition states of gases across graphene nanopore is computed at a critical isovalue of 0.02 e/Å^3 (Figure 6). It can be found that there are some overlaps between the H_2 (He) and strain-free graphene nanopore, whereas the electron overlaps are much more pronounced between the graphene nanopore and other gases (CO_2, O_2, N_2, and CO) at the transition state. With the increasing of strains, these overlaps between gases and graphene nanopores at transition state reduce or disappear, explaining the increasing of permeance because of the reduced size-exclusion effect. Furthermore, the shape of the nanopore changes differently upon applying uniaxial and biaxial strains. The electron charge densities of nanopore under no strain, uniaxial strains, and biaxial strains are shown in Figure S2. Furthermore, the sizes of the nanopore that are defined as the area (diameter) of maximum incircle in the nanopore, respectively, are calculated for analysis. As shown in Figure 7a, the sizes of the nanopore increase with the increasing strain. The sizes of the nanopore under the biaxial strain of 5% are larger than those under the uniaxial strain of 10%, which agree with the results of the transport rates. As shown in Figure 7a, the nanopores deform more uniformly when biaxial strains applied than when uniaxial strains are applied, thus resulting in a more pronounced improvement of gas permeance by biaxial strain engineering. As shown in Figure 7b, it is interesting that the barrier of N_2 is larger than that of the CO, while the kinetic diameter of N_2 is slightly smaller than that of CO. The underlying mechanism can be found in Figure S3, which demonstrates that there is a geometry distortion as CO passes through the nanopore that reduces the energy barrier, resulting from the asymmetric configuration of CO compared with that of N_2. It suggests that the configurations of gases also influence the transport performance across the nanopore.

3.4. Additional Remarks. The experimental realization of strain-engineered nanoporous graphene is challenging; however, here we propose some potential approaches based on recent experimental advances. First, the nanoporous graphene for gas separation is usually placed on the substrate, and the mechanical strains can be applied to the substrate by directly stretching, or bending-induced stretching the substrate and thus transferring the loading into the graphene. Second, the strain engineering of nanoporous graphene can be realized by applying different pressures in the selective gas separation process. These approaches have been successfully applied for the precise strain engineering of two-dimensional materials.[47,48]

Furthermore, the size, shape, and density of graphene nanopores in practical uses can be different from the specific structures explored in this work (0.63 pores/nm^2), which can affect the separation and mechanical performance of nanoporous graphene.[49−51] For example, the nanopore density has dual roles in the nanoporous graphene: It weakens the mechanical properties of graphene but increases the effective area for gas separation. Hence, it is expected that there is an optimal nanopore density to maximize gas separation perform-

https://dx.doi.org/10.1021/acsanm.0c02340
ACS Appl. Nano Mater. 2020, 3, 11474−11480

ance. To address these issues, advanced techniques are needed for precisely fabricating uniform and finely defined nanopores. Fortunately, remarkable advances in fabricating nanopores in graphene using the etching method have recently been achieved.[52−54] Finally, it should be noted that although our work used graphene as a testbed to demonstrate the concept of strain-engineered nanopores for selective gas separation, it is expected that this strain engineering strategy can be used for other 2D materials or gases.

4. CONCLUSIONS

In summary, the gas separation performance of nanoporous graphene under a wide range of mechanical loads is investigated combining first-principles calculations and transition state theory. It is found that the mechanical loads can efficiently regulate the permeance and selectivity of the nanoporous graphene. With the increasing of mechanical strains, the strain-engineered nanopores exhibit remarkably improved permeance while maintaining significant selectivity for gas separation, suggesting the mechanosensitive nanopores for selective gas separation. Our findings demonstrate that strain engineering is a highly efficient strategy to tune the gas separation performance of nanoporous membranes.

■ ASSOCIATED CONTENT

Supporting Information

The Supporting Information is available free of charge at https://pubs.acs.org/doi/10.1021/acsanm.0c02340.

Bond length of gas molecules and energy barriers, energy profiles, and atomic structures of typical gas molecules passing through the nanoporous graphene under no, uniaxial, and biaxial strains (PDF)

■ AUTHOR INFORMATION

Corresponding Authors

Enlai Gao − *Department of Engineering Mechanics, School of Civil Engineering, Wuhan University, Wuhan, Hubei 430072, China;* orcid.org/0000-0003-1960-0260; Email: enlaigao@whu.edu.cn

Ning Wei − *Jiangsu Key Laboratory of Advanced Food Manufacturing Equipment and Technology, Jiangnan University, Wuxi 214122, China;* orcid.org/0000-0003-4566-4778; Email: weining@mail.tsinghua.edu.cn

Authors

Chunbo Zhang − *Department of Engineering Mechanics, School of Civil Engineering, Wuhan University, Wuhan, Hubei 430072, China*

Ke Zhou − *State Key Laboratory for Strength and Vibration of Mechanical Structures, School of Aerospace, Xi'an Jiaotong University, Xi'an 710049, China;* orcid.org/0000-0003-2239-4381

Complete contact information is available at: https://pubs.acs.org/10.1021/acsanm.0c02340

Notes

The authors declare no competing financial interest.

■ ACKNOWLEDGMENTS

This work was supported by the Natural Science Foundation of Hubei Province (2019CFB174) and the start-up fund of the Wuhan University. C.Z. acknowledges the technical advice from Zhen Li and Jinxi Hu. The numerical calculations in this work have been done on the supercomputing system in the Supercomputing Center of Wuhan University.

■ REFERENCES

(1) Kerry, F. G., *Industrial Gas Handbook*; CRC Press, 2007; 552 pages.

(2) Ockwig, N. W.; Nenoff, T. M. Membranes for Hydrogen Separation. *Chem. Rev.* **2007**, *107*, 4078−4110.

(3) Nuttall, W. J.; Clarke, R. H.; Glowacki, B. A. Stop Squandering Helium. *Nature* **2012**, *485*, 573−575.

(4) Boot-Handford, M. E.; Abanades, J. C.; Anthony, E. J.; Blunt, M. J.; Brandani, S.; Mac Dowell, N.; Fernandez, J. R.; Ferrari, M. C.; Gross, R.; Hallett, J. P.; Haszeldine, R. S.; Heptonstall, P.; Lyngfelt, A.; Makuch, Z.; Mangano, E.; Porter, R. T. J.; Pourkashanian, M.; Rochelle, G. T.; Shah, N.; Yao, J. G.; Fennell, P. S. Carbon Capture and Storage Update. *Energy Environ. Sci.* **2014**, *7*, 130−189.

(5) Scholes, C. A.; Ghosh, U. K. Review of Membranes for Helium Separation and Purification. *Membranes* **2017**, *7*, 9.

(6) Cardoso, S. P.; Azenha, I. S.; Lin, Z.; Portugal, I.; Rodrigues, A. E.; Silva, C. M. Inorganic Membranes for Hydrogen Separation. *Sep. Purif. Rev.* **2018**, *47*, 229−266.

(7) Galizia, M.; Chi, W. S.; Smith, Z. P.; Merkel, T. C.; Baker, R. W.; Freeman, B. D. 50th Anniversary Perspective: Polymers and Mixed Matrix Membranes for Gas and Vapor Separation: A Review and Prospective Opportunities. *Macromolecules* **2017**, *50*, 7809−7843.

(8) Dong, Q.; Zhang, X.; Liu, S.; Lin, R. B.; Guo, Y.; Ma, Y.; Yonezu, A.; Krishna, R.; Liu, G.; Duan, J.; Matsuda, R.; Jin, W.; Chen, B. Tuning Gate-Opening of a Flexible Metal-Organic Framework for Ternary Gas Sieving Separation. *Angew. Chem., Int. Ed.* **2020**, *59*, 2−9.

(9) Duan, J. G.; Li, Y. S.; Pan, Y. C.; Behera, N.; Jin, W. Q. Metal-Organic Framework Nanosheets: An Emerging Family of Multifunctional 2D Materials. *Coord. Chem. Rev.* **2019**, *395*, 25−45.

(10) Dong, Q.; Guo, Y.; Cao, H.; Wang, S.; Matsuda, R.; Duan, J. Accelerated C_2H_2/CO_2 Separation by a Se-Functionalized Porous Coordination Polymer with Low Binding Energy. *ACS Appl. Mater. Interfaces* **2020**, *12*, 3764−3772.

(11) Yampolskii, Y. Polymeric Gas Separation Membranes. *Macromolecules* **2012**, *45*, 3298−3311.

(12) Bernardo, P.; Drioli, E.; Golemme, G. Membrane Gas Separation: A Review/State of the Art. *Ind. Eng. Chem. Res.* **2009**, *48*, 4638−4663.

(13) Yuan, W. J.; Chen, J.; Shi, G. Q. Nanoporous Graphene Materials. *Mater. Today* **2014**, *17*, 77−85.

(14) Zhao, Y.; Xie, Y.; Liu, Z.; Wang, X.; Chai, Y.; Yan, F. Two-Dimensional Material Membranes: An Emerging Platform for Controllable Mass Transport Applications. *Small* **2014**, *10*, 4521−4542.

(15) Gadipelli, S.; Guo, Z. X. Graphene-Based Materials: Synthesis and Gas Sorption, Storage and Separation. *Prog. Mater. Sci.* **2015**, *69*, 1−60.

(16) Moghadam, F.; Park, H. B. 2D Nanoporous Materials: Membrane Platform for Gas and Liquid Separations. *2D Mater.* **2019**, *6*, No. 042002.

(17) Chen, B.; Jiang, H. F.; Liu, H. D.; Liu, K.; Liu, X.; Hu, X. J. Thermal-Driven Flow inside Graphene Channels for Water Desalination. *2D Mater.* **2019**, *6*, No. 035018.

(18) Bunch, J. S.; Verbridge, S. S.; Alden, J. S.; van der Zande, A. M.; Parpia, J. M.; Craighead, H. G.; McEuen, P. L. Impermeable Atomic Membranes from Graphene Sheets. *Nano Lett.* **2008**, *8*, 2458−2462.

(19) Berry, V. Impermeability of Graphene and Its Applications. *Carbon* **2013**, *62*, 1−10.

(20) Leenaerts, O.; Partoens, B.; Peeters, F. M. Graphene: A Perfect Nanoballoon. *Appl. Phys. Lett.* **2008**, *93*, No. 193107.

(21) Jiang, D. E.; Cooper, V. R.; Dai, S. Porous Graphene as the Ultimate Membrane for Gas Separation. *Nano Lett.* **2009**, *9*, 4019−4024.

(22) Xie, G.; Yang, R.; Chen, P.; Zhang, J.; Tian, X.; Wu, S.; Zhao, J.; Cheng, M.; Yang, W.; Wang, D.; He, C.; Bai, X.; Shi, D.; Zhang, G. A General Route Towards Defect and Pore Engineering in Graphene. *Small* **2014**, *10*, 2280−2284.
(23) Koenig, S. P.; Wang, L.; Pellegrino, J.; Bunch, J. S. Selective Molecular Sieving through Porous Graphene. *Nat. Nanotechnol.* **2012**, *7*, 728−732.
(24) Zhou, D.; Cui, Y.; Xiao, P. W.; Jiang, M. Y.; Han, B. H. A General and Scalable Synthesis Approach to Porous Graphene. *Nat. Commun.* **2014**, *5*, No. 4716.
(25) Jiao, Y.; Du, A.; Hankel, M.; Zhu, Z.; Rudolph, V.; Smith, S. C. Graphdiyne: A Versatile Nanomaterial for Electronics and Hydrogen Purification. *Chem. Commun.* **2011**, *47*, 11843−11845.
(26) Peng, Y.; Li, Y.; Ban, Y.; Jin, H.; Jiao, W.; Liu, X.; Yang, W. Membranes. Metal-Organic Framework Nanosheets as Building Blocks for Molecular Sieving Membranes. *Science* **2014**, *346*, 1356−1359.
(27) Dai, Z. H.; Liu, L. Q.; Zhang, Z. Strain Engineering of 2D Materials: Issues and Opportunities at the Interface. *Adv. Mater.* **2019**, *31*, No. 1805417.
(28) Li, Y.; Wang, T. M.; Wu, M.; Cao, T.; Chen, Y. W.; Sankar, R.; Ulaganathan, R. K.; Chou, F. C.; Wetzel, C.; Xu, C. Y.; Louie, S. G.; Shi, S. F. Ultrasensitive Tunability of the Direct Bandgap of 2D InSe Flakes Via Strain Engineering. *2D Mater.* **2018**, *5*, No. 021002.
(29) Silva-Guillén, J. A.; Canadell, E. Strain Control of the Competition between Metallic and Semiconducting States in Single-Layers of $TaSe_3$. *2D Mater.* **2020**, *7*, No. 025038.
(30) Kresse, G.; Hafner, J. Ab Initio Molecular-Dynamics Simulation of the Liquid-Metal-Amorphous-Semiconductor Transition in Germanium. *Phys. Rev. B* **1994**, *49*, 14251−14269.
(31) Kresse, G.; Furthmuller, J. Efficient Iterative Schemes for Ab Initio Total-Energy Calculations Using a Plane-Wave Basis Set. *Phys. Rev. B* **1996**, *54*, 11169−11186.
(32) Blöchl, P. E. Projector Augmented-Wave Method. *Phys. Rev. B* **1994**, *50*, 17953−17979.
(33) Perdew, J. P.; Burke, K.; Ernzerhof, M. Generalized Gradient Approximation Made Simple. *Phys. Rev. Lett.* **1996**, *77*, 3865−3868.
(34) Monkhorst, H. J.; Pack, J. D. Special Points for Brillouin-Zone Integrations. *Phys. Rev. B* **1976**, *13*, 5188−5192.
(35) Grimme, S.; Antony, J.; Ehrlich, S.; Krieg, H. A Consistent and Accurate Ab Initio Parametrization of Density Functional Dispersion Correction (DFT-D) for the 94 Elements H-Pu. *J. Chem. Phys.* **2010**, *132*, No. 154104.
(36) Henkelman, G.; Uberuaga, B. P.; Jonsson, H. A Climbing Image Nudged Elastic Band Method for Finding Saddle Points and Minimum Energy Paths. *J. Chem. Phys.* **2000**, *113*, 9901−9904.
(37) Kozuch, S.; Shaik, S. How to Conceptualize Catalytic Cycles? The Energetic Span Model. *Acc. Chem. Res.* **2011**, *44*, 101−110.
(38) Ambrosetti, A.; Silvestrelli, P. L. Gas Separation in Nanoporous Graphene from First Principle Calculations. *J. Phys. Chem. C* **2014**, *118*, 19172−19179.
(39) Blankenburg, S.; Bieri, M.; Fasel, R.; Mullen, K.; Pignedoli, C. A.; Passerone, D. Porous Graphene as an Atmospheric Nanofilter. *Small* **2010**, *6*, 2266−2271.
(40) Li, Y.; Zhou, Z.; Shen, P.; Chen, Z. Two-Dimensional Polyphenylene: Experimentally Available Porous Graphene as a Hydrogen Purification Membrane. *Chem. Commun.* **2010**, *46*, 3672−3674.
(41) Li, J. R.; Kuppler, R. J.; Zhou, H. C. Selective Gas Adsorption and Separation in Metal-Organic Frameworks. *Chem. Soc. Rev.* **2009**, *38*, 1477−1504.
(42) Wang, Y.; Li, J.; Yang, Q.; Zhong, C. Two-Dimensional Covalent Triazine Framework Membrane for Helium Separation and Hydrogen Purification. *ACS Appl. Mater. Interfaces* **2016**, *8*, 8694−8701.
(43) Logan, S. R. The Origin and Status of the Arrhenius Equation. *J. Chem. Educ.* **1982**, *59*, 279−281.
(44) Yuan, Z.; Govind Rajan, A.; Misra, R. P.; Drahushuk, L. W.; Agrawal, K. V.; Strano, M. S.; Blankschtein, D. Mechanism and Prediction of Gas Permeation through Sub-Nanometer Graphene Pores: Comparison of Theory and Simulation. *ACS Nano* **2017**, *11*, 7974−7987.
(45) Yao, B.; Mandra, S.; Curry, J. O.; Shaikhutdinov, S.; Freund, H. J.; Schrier, J. Gas Separation through Bilayer Silica, the Thinnest Possible Silica Membrane. *ACS Appl. Mater. Interfaces* **2017**, *9*, 43061−43071.
(46) Singh, A.; Koros, W. J. Significance of Entropic Selectivity for Advanced Gas Separation Membranes. *Ind. Eng. Chem. Res.* **1996**, *35*, 1231−1234.
(47) Wang, G.; Dai, Z.; Wang, Y.; Tan, P.; Liu, L.; Xu, Z.; Wei, Y.; Huang, R.; Zhang, Z. Measuring Interlayer Shear Stress in Bilayer Graphene. *Phys. Rev. Lett.* **2017**, *119*, No. 036101.
(48) Wang, G. R.; Gao, E. L.; Dai, Z. H.; Liu, L. Q.; Xu, Z. P.; Zhang, Z. Degradation and Recovery of Graphene/Polymer Interfaces under Cyclic Mechanical Loading. *Compos. Sci. Technol.* **2017**, *149*, 220−227.
(49) Lee, C. K.; Hwangbo, Y.; Kim, S. M.; Lee, S. K.; Lee, S. M.; Kim, S. S.; Kim, K. S.; Lee, H. J.; Choi, B. I.; Song, C. K.; Ahn, J. H.; Kim, J. H. Monatomic Chemical-Vapor-Deposited Graphene Membranes Bridge a Half-Millimeter-Scale Gap. *ACS Nano* **2014**, *8*, 2336−2344.
(50) Liu, Y. L.; Chen, X. Mechanical Properties of Nanoporous Graphene Membrane. *J. Appl. Phys.* **2014**, *115*, No. 034303.
(51) Gao, E.; Cao, Y.; Liu, Y.; Xu, Z. Optimizing Interfacial Cross-Linking in Graphene-Derived Materials, Which Balances Intralayer and Interlayer Load Transfer. *ACS Appl. Mater. Interfaces* **2017**, *9*, 24830−24839.
(52) Yang, Y.; Yang, X.; Liang, L.; Gao, Y.; Cheng, H.; Li, X.; Zou, M.; Ma, R.; Yuan, Q.; Duan, X. Large-Area Graphene-Nanomesh/Carbon-Nanotube Hybrid Membranes for Ionic and Molecular Nanofiltration. *Science* **2019**, *364*, 1057−1062.
(53) Choi, K.; Droudian, A.; Wyss, R. M.; Schlichting, K. P.; Park, H. G. Multifunctional Wafer-Scale Graphene Membranes for Fast Ultrafiltration and High Permeation Gas Separation. *Sci. Adv.* **2018**, *4*, No. eaau0476.
(54) Zhao, J.; He, G.; Huang, S.; Villalobos, L. F.; Dakhchoune, M.; Bassas, H.; Agrawal, K. V. Etching Gas-Sieving Nanopores in Single-Layer Graphene with an Angstrom Precision for High-Performance Gas Mixture Separation. *Sci Adv* **2019**, *5*, No. eaav1851.

https://dx.doi.org/10.1021/acsanm.0c02340
ACS Appl. Nano Mater. 2020, 3, 11474−11480

Supporting Information for

A Computational Study on Strain-Engineered Graphene Nanopores for Selective Gas Separation

Enlai Gao[1*], Chunbo Zhang[1], Ke Zhou[2], and Ning Wei[3*]

[1]Department of Engineering Mechanics, School of Civil Engineering, Wuhan University, Wuhan, Hubei 430072, China.

[2]State Key Laboratory for Strength and Vibration of Mechanical Structures, School of Aerospace, Xi'an Jiaotong University, 710049, Xi'an, China

[3]Jiangsu Key Laboratory of Advanced Food Manufacturing Equipment and Technology, Jiangnan University, 214122 Wuxi, China.

[*]Corresponding author. Email: enlaigao@whu.edu.cn; weining@mail.tsinghua.edu.cn

This Supporting Information contains

- **Tables S1-S2.**
- **Figures S1-S3.**

Table S1. Calculated bond length of molecules as compared with that from literature (unit: Å).

	H_2	O_2	CO_2	CO	N_2
This work	0.751	1.233	1.177	1.143	1.113
LDA	-	1.223[a]	-	1.138[a]	1.109[a]
PW91	-	1.237[a]	-	1.145[a]	1.113[a]
PW91PW91/6-31G	-	1.228[a]	-	1.148[a]	1.116[a]
PBE	0.750[b]	-	-	-	-
Exp.	0.741[c]	1.208[d]	1.163[e]	1.128[f]	1.098[g]

Ref [a] Taken from Ref.[1]
Ref [b] Taken from Ref.[2]
Ref [c] Taken from Ref.[3]
Ref [d] Taken from Ref.[4]
Ref [e] Taken from Ref.[5]
Ref [f] Taken from Ref.[6]
Ref [g] Taken from Ref.[7]

Table S2. Potential energy barriers (eV) of gases passing through the nano-porous graphene, under free, uniaxial strains of 5% and 10% along the armchair direction, and biaxial strains of 5% and 10%, respectively.

Gases/strains	He	H_2	O_2	CO_2	CO	N_2
0%	0.41	0.54	1.01	1.82	2.09	2.35
ε_x=5%	0.28	0.32	0.75	1.30	1.53	1.71
ε_x=10%	0.17	0.22	0.44	0.88	1.01	1.13
ε_x=ε_y=5%	0.13	0.17	0.32	0.78	0.89	0.99
ε_x=ε_y=10%	0.03	0.02	0.09	0.32	0.30	0.34

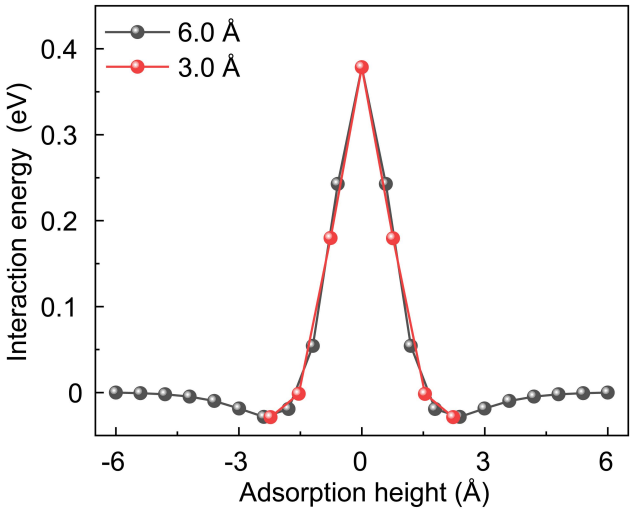

Figure S1. Energy profile for a He atom passing through the graphene nanopores. The red and the black data are the paths of He across the nanopores with initial configurations of He atom 3.0 Å and 6.0 Å from graphene plane before optimization (the initial height of 3.0 Å slightly changes to the optimal adsorption height while the initial height of 6.0 Å almost does not change upon the optimization of these two initial configurations), respectively.

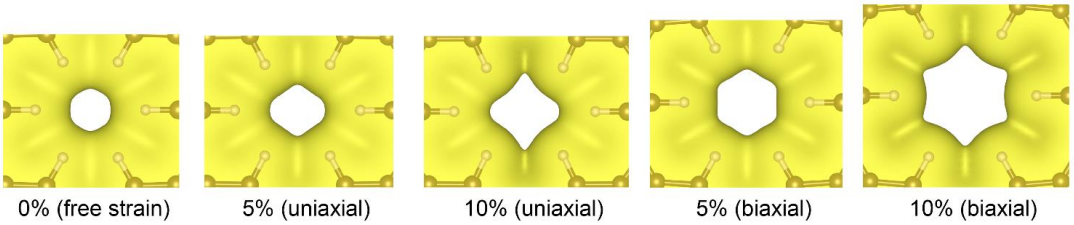

Figure S2. Top view of electron charge densities of nanopore under free, uniaxial and biaxial strains, in which the iso-surface value is adopted as 0.02 e/Å^3.

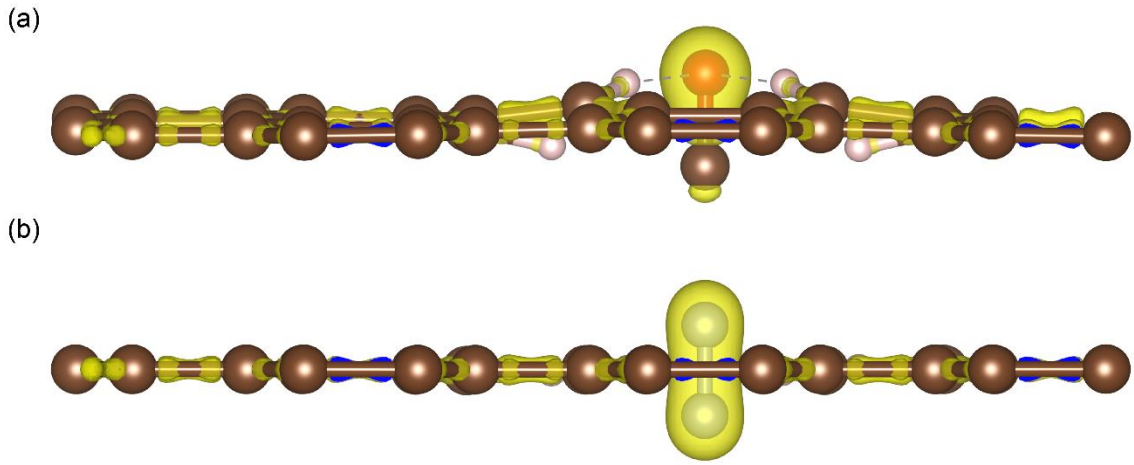

Figure S3. Side view of electron charge densities of (a) CO and (b) N_2 passing through the strain free porous graphene at transition state, respectively.

References:

(1) Sun G. Y.; Kurti J.; Rajczy P.; Kertesz M.; Hafner J.; Kresse G. Performance of the Vienna ab initio simulation package (VASP) in chemical applications. *J. Mol. Struct.* **2003,** *624*, 37-45.

(2) Li S.; Yu A.; Toledo F.; Han Z.; Wang H.; He H. Y.; Wu R.; Ho W. Rotational and vibrational excitations of a hydrogen molecule trapped within a nanocavity of tunable dimension. *Phys. Rev. Lett.* **2013,** *111*, 146102.

(3) Herzberg G H. K. P. Molecular spectra and molecular structure. IV. Constants of diatomic molecules. **1979,** Van Nostrand Reinhold Co..

(4) Herzberg G. Molecular spectra and molecular structure I, spectra of diatomics molecules. **1953,** Van Nostrand: Toronto.

(5) Greenwood N. N.; Earnshaw A. Chemistry of the elements. **1997,** Butterworth-Heinemann: Oxford.

(6) Mantz A. W.; Watson J. K. G.; Rao K. N.; Albritton D. L.; Schmeltekopf A. L.; Zare R. N. Rydberg-Klein-Rees potential for the $X^1\Sigma+$ state of the CO molecule. *J. Mol. Spectrosc.* **1971,** *39*, 180-184.

(7) Huber K.-P.; Herzberg G. Constants of diatomic molecules. **1979,** Van Nostrand: Princeton.